JPCE

Journal de physique et de chimie des étudiants

Numéro 4 - 24 mai 2021
Pages 94 - 111

Sciences de la Matière

Electrodynamics of Pulsars

B. Crinquand

This article aims at describing the physics of pulsars. After figuring the nature of pulsars through observational data, emphasis is laid on the importance of pulsar magnetospheres in this problem. The question of pulsar energy loss is then tackled, by means of a few approximations.

1. Introduction

Neutron stars are fascinating objects, possessing both huge electromagnetic and gravitational fields. Interest in their study has been revived by the discovery of pulsars, a sub-class of neutron stars emitting pulses at a very stable rate. Pulsars have made many progresses in observational high-energy physics and astrophysics possible. However, although the very nature of a pulsar is fairly simple, the basic properties of pulsar emission are still not fully understood. The purpose of this article is to review the properties of pulsar magnetospheres, starting from the basics. The nature of pulsars is introduced in Section 2, as well as a quick description of the emission problem. The physics at play in pulsar magnetospheres is outlined in Section 3, whereas qualitative and quantitative solutions of this problem are analyzed in Section 4.

2. About pulsars

In this section, the properties of pulsars are deduced from observations.

2.1. The discovery of pulsars

Anthony Hewish, an astronomer at the university of Cambridge, launched during the 60's a radio observational study of the interstellar medium, his prime objective being the discovery of quasars. 2048 radio dipole antennae were set over four and a half acres of English countryside. His PhD student Jocelyn Bell observed in 1967 important fluctuations, "scruff", in the signal detected by the radio telescope (Figure 1). Careful measurements showed that the source passed over her fixed array of antennae every sidereal day, indicating that the source was among the stars rather than in the Solar System. Using a faster recorder she realized that the scruff consisted of a series of regularly spaced radio pulses $1,337$ s apart.[1] At that time, such a precise celestial clock was unheard of. These radio sources were named "pulsars". Hewish was awarded a Nobel Prize in 1974 for this discovery but Bell did not, although she was the first to notice the signal. This controversial omission has later been referred to as the "No-Bell" prize. Nowadays more than 2000 pulsars are known.

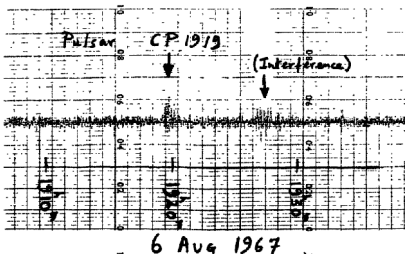

Fig. 1 Observation notes from Jocelyn Bell, showing the scruff caused by pulsar PSR B1919+21. "CP" stands for Cambridge Pulsar. Figure taken from [1].

Pulses are generally brief and received over a small fraction of the pulsar period. As can be seen on Figure 2, one pulse consists of a number of brief subpulses. Although their shape varies substantially from one to another, the integrated pulse profile proves very stable. The discovery of pulsars has been a major upheaval in astrophysics. Aside from raising theoretical problems, radio pulsars are used for astrophysical measurements, due to the possibility to control both the frequency and the phase of the signal. We can mention, among others:

- the measure of electron density in the interstellar medium (Figure 3);
- the determination of the galactic magnetic field from the polarization plane rotation at different frequencies thanks to the Faraday effect;[2]
- on a more theoretical point of view, the study of quantum processes in strong magnetic fields;
- the detection of gravitational waves through extremely precise timing measurements. The European Pulsar Timing Array is dedicated to this task (some additional information is available at http://www.epta.eu.org/).

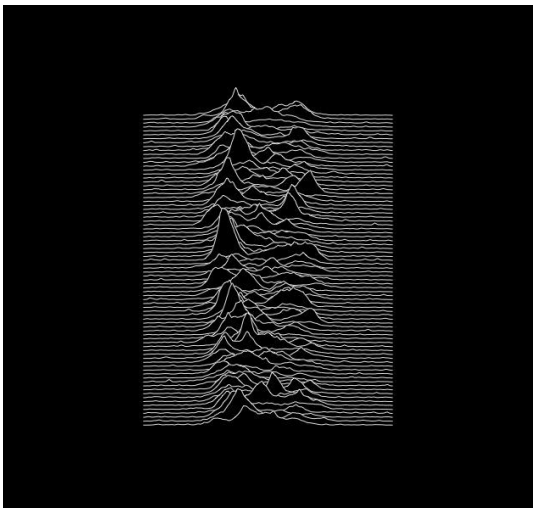

Fig. 2 Artwork of the album *Unknown Pleasures*, released in 1979 by the English band Joy Division, based on an image of radio waves from the first pulsar discovered PSR B1919+21. The name of the pulsar contains its right ascension and declination, whereas "PSR" stands for Pulsating Source of Radio.

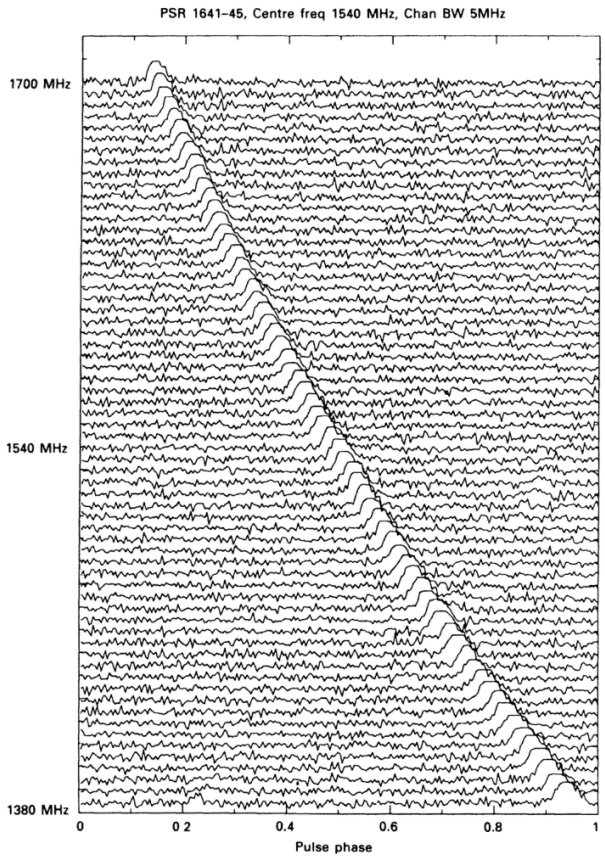

Fig. 3 Pulse phase for different frequencies in the radio domain for pulsar PSR 1641-45. Waves propagating at lower frequencies are subjected to greater dispersion, increasing the phase delay. Besides, more distant pulsars exhibit a greater pulse disperion, which can be used to measure distances to pulsars. Figure taken from [1].

2.2. The nature of pulsars

All known pulsars share a common set of characteristics, which give important clues as to the nature of these objects. Most pulsars have periods P ranging from 0.25 s to 2 s. The fastest pulsars have periods around the millisecond. They are thought to be "recycled" pulsars, that were spun up through accretion of matter from a companion in a binary system. Their periods are extremely well defined on the scale of a year, and the precision of these measurements challenges the accuracy of atomic clocks. This stability makes them extremely sensitive to their environments: objects orbiting around pulsars can be detected thanks to the Doppler shift in their pulses. The first confirmed exoplanets were discovered using this method. More importantly, the periods of all pulsars *increase* gradually as pulsars slow down. The rate of increase is typically $\dot{P} \approx 10^{-15}$ s/s. This

yields an order of magnitude for the lifetime of pulsars $\tau \sim P/\dot{P}$ of several million years. Several hypotheses were made to account for these observations, assuming the pulsar period is related to some physical periodic phenomenon.

- **A binary system** If the orbital periods of a binary star system is involved, then those stars must be extremely compact. Indeed, the orbital period of such a system is bounded by[3]

$$P > \sqrt{\frac{3\pi}{\rho G}}, \tag{1}$$

where ρ is the density of the stars and G the gravitational constant. This corresponds to the minimal achievable period, both stars being as close as possible given their radius. For instance, a typical white dwarf has $\rho \approx 10^9\,\mathrm{kg\cdot m^{-3}}$, so that $P > 10$ s, far from the observed millisecond pulsars. On the other hand, neutron stars are so small and compact that this could be compatible with the observed periods. However, two neutron stars rapidly orbiting would generate intense gravitational waves[4] and lose their energy. This would lead to a decrease in their period, rather than an increase. The possibility of a binary system is ruled out.

- **Pulsating stars** The oscillation period of a star can be shown to be proportional to $1/\sqrt{\rho}$,[1] just like the adiabatic speed of sound in a fluid. For white dwarfs this yields periods between 100 and 1000 s whereas neutron stars would have a fundamental radial mode oscillating at 10^{-4} s. Neither corresponds to the observed periods.

- **Rotating stars** The angular velocity of a star of mass M and radius R is limited by the ability of gravity to counterbalance the centrifugal acceleration. This constraint is most severe at the equator. Assuming a spherical star despite its rotation, the maximum angular velocity Ω can be found by writing

$$\Omega_{\max}^2 R = \frac{GM}{R^2} \Rightarrow P_{\min} = 2\pi\sqrt{\frac{R^3}{GM}}. \tag{2}$$

This is too long for red giants or white dwarfs, but for a $1,4\ M_\odot$ neutron star we would have $P \approx 5 \times 10^{-4}$ s, which accommodates the complete range of pulsar periods.[3]

All in all, a pulsar can only be a very rapidly rotating neutron star.

2.3. An aside on neutron stars

Neutron stars result from the collapse of ordinary massive stars at the later stage of their evolution. Stars with mass inferior to the Chandrasekhar limit $M_{\mathrm{Ch}} = 1.4\ M_\odot$ turn quietly into white dwarves with no collapse. Because neutron stars are formed when the degenerate core of an aging supergiant star reaches the Chandrasekhar limit, we take M_{Ch} to be the mass of a typical neutron star.[1] Gravity in a neutron star is supported by neutron degeneracy pressure,[5] which requires the radius of the neutron star to be around 10 km. A precise measurement of the radius of a neutron star is still lacking, and would be incredibly useful to determine the equation of state of matter inside the star. The NICER mission[6] aims at determining a pulsar radius by fitting X-ray lightcurves.

This allows us to interpret the small rotation period. Treating each star as a sphere, conservation of angular momentum implies

$$M_i R_i^2 \Omega_i = M_f R_f^2 \Omega_f, \tag{3}$$

the subscript "i" (resp. "f") denoting the initial (resp. final) state of the star, M being its mass, R its radius and Ω its angular velocity. White dwarves have radii around 10^3 km. The question of how fast the progenitor core may be rotating is harder to answer. Since the core is not isolated from its envelope as the star evolves, conservation of angular momentum cannot be used so recklessly. Measurements of rotation periods yield $P_i \approx 10^3$ s, so the post-collapse neutron star can rotate as fast as 10^{-3} s.

Besides, it should be mentioned that the interior of neutron stars, albeit not completely understood as of today, is an excellent conductor. Let us briefly explain why. The density of a neutron star is immense: it is typically $\rho_{ns} \approx 10^{17}\,\mathrm{kg\cdot m^{-3}}$, of the same order of magnitude than the density of an atomic nucleus,[7] just like if the neutrons were "touching" each other. So we need to consider the lowest energy configuration of a mixture of about 10^{57} nucleons with enough free degenerate electrons to provide zero net charge. Initially,

at low densities, nucleons are found confined in iron nuclei. This is the outcome of a compromise between the repulsive Coulomb force and the attractive nuclear force between nucleons. However, as ρ increases, electrons become relativistic and start to convert protons in the nuclei into neutrons by an electron capture process:

$$p + e^- \rightarrow n + \nu_e. \tag{4}$$

This reaction is allowed if the kinetic energy of the electron makes up for the difference in rest mass energy: $(m_n - m_p - m_e)c^2 = 0.78\,\mathrm{MeV}$. This process is called neutronization: the nuclei forming the star get richer and richer in neutrons as ρ increases. The inverse β^- decay is not allowed since, under the conditions of complete electron degeneracy, there are no vacant states available for an emitted electron to occupy. At even higher densities, as the density reaches that of a nucleus, neutrons are no longer confined into nuclei and free neutrons appear, forming a superfluid. Similarly, the remaining free protons pair up and form a superconducting fluid. The ratio neutrons/protons, electrons reaches a limiting value of 8/1 determined by the competition between electron capture and β decay. So the interior of a neutron star is close to a perfect conductor.

2.4. Connection with nebulae

The interpretation of pulsars as rotating neutron stars was strengthened by the discovery of a very fast pulsar with $P = 0.0333$ s and $\dot{P} = 4.21 \times 10^{-13}$ within the Crab nebula, a supernova remnant. The Crab nebula is a remnant of the 1054 supernova, recorded by Chinese astronomers. The nebula was the first astronomical object identified with a historical supernova explosion. A nebula is an interstellar cloud of dust, hydrogen, helium and other ionized gases. Some nebulae form as the result of supernova explosions. The material thrown away is ionized by the energy of the compact object its core produces. This is the case for the Crab nebula. Some form from the gas that is already in the interstellar medium, like giant molecular clouds. Some others result from the expanding, glowing shell of ionized gas ejected from red giants at the final stage of their lives, like the Cat's nebula. Note that the Crab pulsar not only produces radio bursts, but pulses in a whole electromagnetic spectrum ranging from radio to gamma rays, including flashes in visible light, as can be seen in Figure 4.

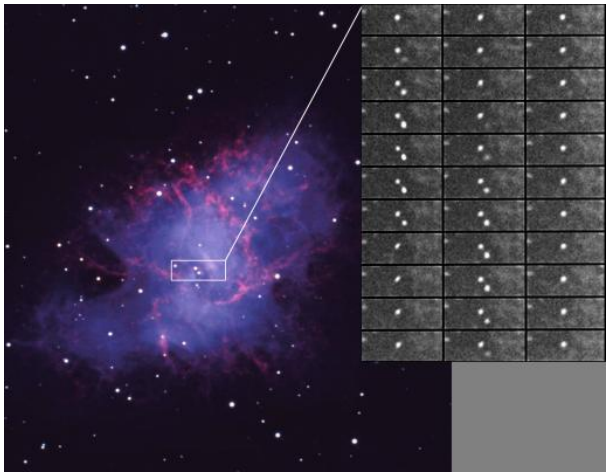

Fig. 4 A sequence of images showing flashes at visible wavelengths from the Crab pulsar. The frequency of the optical pulse is around 30 Hz, in accordance with the pulsar period (Courtesy of NASA).

Observations of the Crab nebula[8] clearly reveal its connection with the pulsar inside it (Figure 5). If the present rate of expansion is extrapolated backward in time, the initial supernova should have occurred about 90 years after the explosion was observed in the sky. This means that the expansion of the nebula must have been accelerating. Besides, it was suggested in 1953 that the light emitted by the nebula might be synchrotron radiation produced when electrons spiral along magnetic field lines. This was confirmed by the polarization of such light. The identification of the white glow with synchrotron radiation means that some weak magnetic field must permeate the nebula. This is puzzling, since the expansion of the nebula should have weakened the magnetic field. This assertion will be justified in Appendix 7.2. It is a consequence of the conservation of magnetic flux. Furthermore, the electrons should have radiated away all of their energy after only 100 years. This implies that the production of synchrotron radiation nowadays requires continuous injection of energetic electrons and supplying of magnetic field. The total power needed for these processes can be estimates to be about 5×10^{31} W.[9] It turns out the energy source is the pulsar at the heart of the Crab nebula, which stores an immense amount of kinetic energy that is supplied as the star slows down. The mechanism causing this slowdown is the topic of Sec-

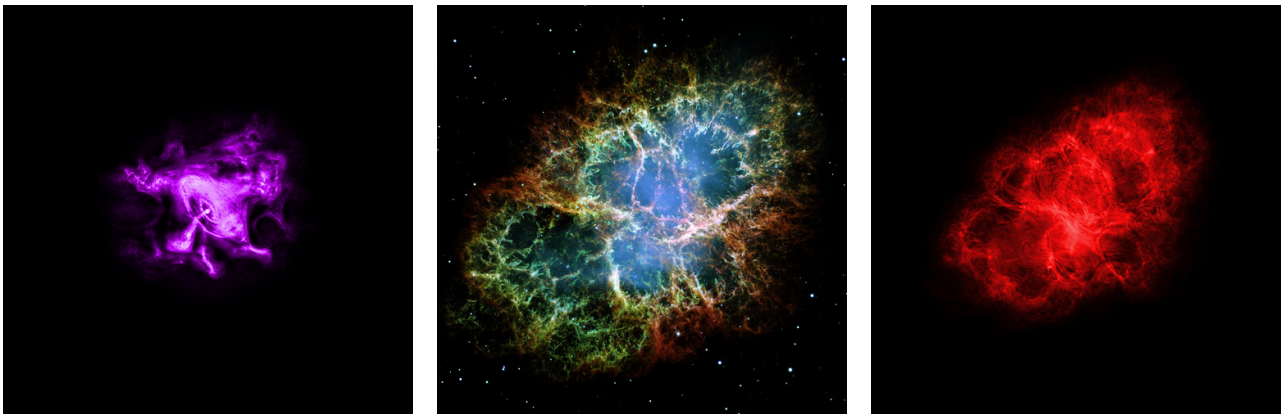

(a) **(b)** **(c)**

Fig. 5 **(a)** X-ray image of the Crab nebula, observed by the Chandra-X-ray Observatory. The pulsar is clearly visible in the middle; there seems to be two antipodal X-ray jets (Courtesy of NASA). **(b)** Image of the Crab nebula in visible light, observed by Hubble Space Telescope. Hydrogen shines in orange, neutral oxygen in blue and singly ionized sulfur in green. The white glow in the middle comes from synchrotron radiation (Courtesy of NASA and ESA). **(c)** Radio image of the Crab nebula observed by the Very Large Array (VLA) (Courtesy of NRAO).

tion 3. In order to check the validity of this assumption let us calculate the rate of energy loss. The kinetic energy of the pulsar is given by

$$E_c = \frac{1}{2} I \Omega^2 = \frac{2\pi^2 I}{P^2}, \tag{5}$$

where $I = 2MR^2/5$ is the moment of inertia of a sphere,[10] so that the rate of energy loss is

$$\frac{\mathrm{d}E_c}{\mathrm{d}t} = -\frac{4\pi^2 I \dot{P}}{P^3}. \tag{6}$$

Assuming the pulsar to be spherical, with $M = 1.4\ M_\odot$ and $R = 10$ km, we get $\mathrm{d}E_c/\mathrm{d}t \approx 5.0 \times 10^{31}$ W. Remarkably, this is exactly the energy required to power the nebula. However, it is important to realize that the radio luminosity of a pulsar only accounts for a very small fraction of its total energy loss.

2.5. Emission mechanism

We still lack a key ingredient, highlighted in the previous subsection: how does the neutron star at the core of the Crab nebula feed the the nebula? Another property of neutron stars that we have not mentioned so far is their huge magnetic field. This is a consequence of the freezing of magnetic field lines in an extremely conducting fluid, which will be proved in Appendix 7.2. The magnetic flux through the surface of a collapsing white dwarf will be conserved. To provide an order of magnitude, ignoring the precise configuration of the magnetic field B, conservation of magnetic flux yields

$$4\pi R_i^2 B_i = 4\pi R_f^2 B_f. \tag{7}$$

A typical white dwarf magnetic field is about 10^2 T, so that the typical magnetic field of a neutron star is $B_{ns} \approx 10^8$ T. For comparison, the highest magnetic field that could be created in laboratory was about 100 T or so. The magnetic field configuration is readily modeled as a magnetic dipole. In the end, a pulsar is but a magnetic dipole rotating very quickly around its rotation axis. Importantly, the rotation axis and the magnetic dipole are usually not aligned. This important feature is responsible for the pulsed emission, as seen from Earth. Knowing that an oscillating magnetic moment radiates, it seems plausible that magnetodipole radiation is responsible for the energy loss of the pulsar. This hypothesis will be examined in Section 3.1.

If the general pattern of pulsar activity seems to have been established, some fundamental problems persist.[11] The point is that the initial hypothesis for the magnetic dipole energy loss mechanism is unrealistic. For instance, low frequency waves with frequency $\nu = 1/P$ cannot propagate into the interstellar medium, that has a typical plasma frequency of several kHz.[2] Another serious theoretical problem is that a bright, low

frequency source from a tiny object exceeds the black body emissivity at any plausible temperature, and has the wrong dependence on frequency (at radio wavelength, the spectral intensity falls with frequency instead of rising). The rotational braking of the star, the associated particle acceleration and transport of energy from the surface up to the nebula therefore all require a detailed knowledge of the pulsar magnetosphere. This will be the topic of Section 3.

3. The physics of pulsar magnetospheres

In this section the topic of pulsar magnetospheres is tackled. We intend to determine the electric and magnetic fields around pulsars and give hints as to why, and to what extent, plasma is involved.

3.1. Vacuum solution

We first discuss a pulsar surrounded with vacuum, even though it is quite unrealistic, as we will soon find out. The initial argument was that strong gravity kept particles in the pulsar atmosphere in the vicinity of the star. This model neglects the lifting of particles by strong induced electric fields. Let us consider a pulsar characterized by its magnetic moment $\boldsymbol{\mathcal{M}}$ and its rotation vector $\boldsymbol{\Omega}$. Let us first consider the case of the "aligned rotator", with parallel $\boldsymbol{\mathcal{M}}$ and $\boldsymbol{\Omega}$. Such a pulsar would not pulsate, and would not even lose energy if we stick to the magnetodipole radiation picture. This study is instructive nonetheless. As mentioned in Section 2.3, neutron stars are excellent conductors. Thus the electric field measured in the rotating frame inside the star must vanish, so that the internal electric field satisfies:

$$\boldsymbol{E}_{\rm int} + \boldsymbol{U} \times \boldsymbol{B} = \boldsymbol{0}, \tag{8}$$

where $\boldsymbol{U} = \boldsymbol{\Omega} \times \boldsymbol{r}$. Since $\boldsymbol{\mathcal{M}}$ is parallel to $\boldsymbol{\Omega}$, the problem is stationary. From this condition we deduce that $\boldsymbol{E}_{\rm int} \cdot \boldsymbol{B} = 0$: magnetic field lines are equipotentials for the electric field. Physically the star, embedded in a magnetic field, is polarized by its rotation.[11] Charges are separated by the Lorentz force and redistribute themselves inside the star to create an electric field balancing this force, such that charges drift with velocity:

$$\boldsymbol{U} = \frac{\boldsymbol{E}_{\rm int} \times \boldsymbol{B}}{B^2} = \boldsymbol{\Omega} \times \boldsymbol{r}. \tag{9}$$

This will provide us with a boundary condition for the electric field exterior to the star. The magnetic field created by the point magnetic dipole located at the center of the pulsar is:[12]

$$\boldsymbol{B}(r,\theta,\varphi) = B_0 \left(\frac{R_0}{r}\right)^3 (2\cos\theta\, \boldsymbol{e}_r + \sin\theta\, \boldsymbol{e}_\theta), \tag{10}$$

where $B_0 = \mathcal{M}/4\pi\mu_0 R_0^3$. The polar θ component of $\boldsymbol{E}_{\rm int}$ is $E_{\theta,{\rm int}} = -U_\varphi B_r$, which yields the potential drop with latitude at the pulsar surface:

$$V(R_0,\theta) = V(R_0,0) - \int_0^\theta E_{\theta,{\rm int}} R_0 {\rm d}\theta' \tag{11}$$

$$= V_0 + \Omega R_0^2 B_0 \sin^2\theta. \tag{12}$$

Then Laplace equation must be resolved in the vacuum with this boundary condition, that can be rewritten in terms of Legendre polynomials $\mathcal{P}_n$:

$$\mathcal{P}_2(\cos\theta) = \frac{1}{2}(3\cos^2\theta - 1) \tag{13}$$

$$\Rightarrow V(R_0,\theta) = V_0 + \frac{2}{3}\Omega R_0^2 B_0 - \frac{2\Omega R_0^2 B_0}{3}\mathcal{P}_2(\cos\theta). \tag{14}$$

Hence, the solution for $r \geq R_0$ is written,[13] with the boundary condition $V(r,\theta) \to 0$ for $r \to +\infty$:

$$V(r,\theta) = \left(V_0 + \frac{2}{3}\Omega R_0^2 B_0\right)\frac{R_0}{r} + \Omega R_0^2 B_0 \left(\frac{R_0}{r}\right)^3 \left(\sin^2\theta - \frac{2}{3}\right). \tag{15}$$

The potential V contains a monopole contribution associated to the net charge of the star. We will assume the neutron star is formed with zero charge, so that $V_0 = -2\Omega R_0^2 B_0/3$. The rotation of the star induces a quadrupolar electric field $\boldsymbol{E}_{\rm ext} = -\boldsymbol{\nabla} V$:

$$\boldsymbol{E}_{\rm ext} = \Omega R_0 B_0 \left(\frac{R_0}{r}\right)^4 ((1-3\cos^2\theta)\, \boldsymbol{e}_r - \sin 2\theta\, \boldsymbol{e}_\theta). \tag{16}$$

The radial and orthoradial components of $\boldsymbol{E}_{\rm ext}$ are shown in Figure 6. Even though the potential is continuous at the stellar surface by construction, its derivative is not. From the radial component of the radial internal electric field

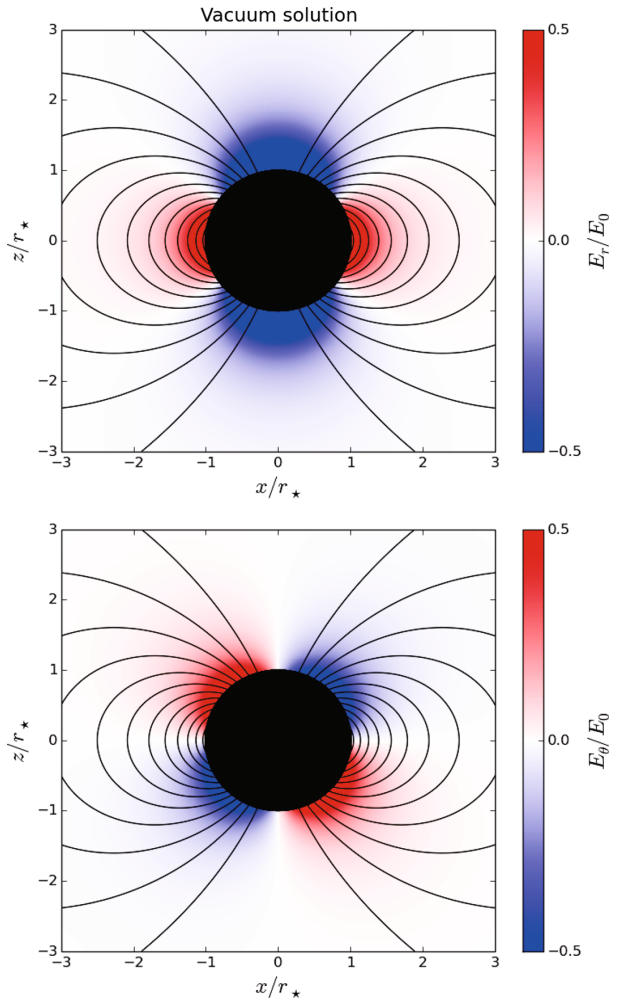

Fig. 6 Radial (up) and polar (down) normalized components of the vacuum electric field $\boldsymbol{E}_{\rm ext}$ of an aligned rotator. The rotation axis is along the z-axis; $r_\star = R_0$ with the notations of this article. Figure taken from [14].

$E_{r,\rm int} = \Omega B_0 R_0 \sin^2\theta$, we get the surface charge density of the star:[14]

$$\sigma = \varepsilon_0 (E_{r,\rm ext} - E_{r,\rm int}) = -2\varepsilon_0 \Omega B_0 R_0 \cos^2\theta. \quad (17)$$

This amounts to a total surface charge $Q_{\rm surf} = -8\pi\varepsilon_0 \Omega B_0 R_0^3/3$. This charge is exactly compensated by the interior charge that can be computed from Gauss theorem applied to a sphere just inside R_0:

$$Q_{\rm int} = \epsilon_0 \int E_{r,\rm int} 2\pi R_0^2 {\rm d}\theta = -Q_{\rm surf}. \quad (18)$$

The net charge of the star thus remains zero. The existence of this surface charge will soon become crucial.

As was mentioned earlier, the aligned rotator does not lose energy and does not spin down. Consider what happens to an inclined rotator:

$$\boldsymbol{\mathcal{M}}(t) = \mathcal{M}(\cos\chi\, \boldsymbol{e}_z + \sin\chi(\cos\Omega t\, \boldsymbol{e}_x + \sin\Omega t\, \boldsymbol{e}_y)), \quad (19)$$

whre χ is the tilt angle between $\boldsymbol{\Omega}$ and $\boldsymbol{\mathcal{M}}(t)$. The power $\mathcal{P}$ radiated away by such a time-dependent magnetic moment can be readily derived:[2,13]

$$\mathcal{P} = \frac{\mu_0}{6\pi c^3} \left| |\ddot{\boldsymbol{\mathcal{M}}}| \right|. \quad (20)$$

This formula can be applied to the special case of Equation 19. A factor of 2 comes out of the presence of two oscillating components, and a factor $1/2$ comes from the time averaging. In the end, the power radiated by an inclined pulsar is

$$\mathcal{P} = \frac{8\pi B_0^2 \Omega^4 R_0^6 \sin^2\chi}{3\mu_0 c^3}. \quad (21)$$

This formula is valid in the vacuum approximation. This energy is drained from the rotational energy of the pulsar: $\mathcal{P} = -I\Omega\dot{\Omega}$. A useful information about the brake efficiency is given by the dimensionless braking index[15]

$$n = \frac{\Omega\ddot{\Omega}}{\dot{\Omega}^2}, \quad (22)$$

corresponding approximately to the exponent of Ω in its slowdown dependence: $\dot{\Omega} \propto -\Omega^n$. Assuming that the magnetic field produced by the star does not decay as the pulsar slows down (or on a much longer scale), a straightforward calculation from Equation 21 gives

$$n = 3 + 2\frac{\Omega}{\dot{\Omega}}\dot{\chi}\cot\chi. \quad (23)$$

A more complete derivation would allow us to calculate the electromagnetic torques exerted by the electromagnetic field on the rotating dipole. It turns out there are components both parallel and orthogonal to the rotation axis,[16] that also tends to reduce the magnetic obliquity. From the components of the Maxwell stress tensor and the components of the magnetic field in the inclined case one can prove that $\Omega\cos\chi$ is a constant of the motion. In the end, the braking index is given by

$$n = 3 + 2\cot^2\chi > 3. \quad (24)$$

This can be compared to observational data. For most radio pulsars, the second derivative of Ω is hard to extract from the noise, but n could be

measured for the fastest pulsars. As can be seen in Table 1, the braking index is always less than 3. Thus we can conclude that the simple magnetodipole mechanism cannot be solely responsible for the pulsar slowdown,[17] as had already pointed out at the end of Section 2.

Pulsar	P	n
B0531 + 21	0.033	2.51 ± 0.01
B0540 - 693	0.050	2.14 ± 0.01
J1119 - 6127	0.408	2.91 ± 0.05
B1509 - 58	0.150	2.84 ± 0.01
J1846 - 0258	0.324	2.65 ± 0.01

Tab. 1 Braking index for fast radio pulsars. Table taken from [17]

3.2. Electrosphere: the presence of plasma

Let us consider the aligned rotator again. Particles are strongly magnetized near the neutron star, with magnetic fields up to 10^8 T, so that their velocities perpendicular to magnetic field lines are limited to the drift velocity $\boldsymbol{U} = \boldsymbol{E} \times \boldsymbol{B}/B^2$. On the other hand, charged particles can freely slide along magnetic field lines if there is an unscreened parallel electric field $E_\parallel = \boldsymbol{E}\cdot\boldsymbol{B}/B$. This is indeed the case in the vacuum solution, out of the star. As we saw earlier, the charge density is nonzero on the stellar surface. The strong magnetic field combined with the rotation of the star generated a potential drop at the surface hardly sustainable for the charges in the crust, so at the surface appears an electric field of the order $E \sim \Omega B_0 R_0 \sim 10^{13}\,\mathrm{V\cdot m^{-1}}$. This huge field extracts charges from the surface despite the presence of a potential barrier due to molecular attraction and despite gravity:

$$\frac{f_{\mathrm{elec}}}{f_{\mathrm{grav}}} = \frac{eER_0^2}{GMm_p} \approx 10^9, \tag{25}$$

even for protons. This is the primary plasma generation. This is true for electrons, but uncertain for ions. However, neutron stars have temperature high enough to generate sufficient ion emission.[18] There exists an axisymmetric electrostatic solution for the lifted charge.[14] The electrons lifted in the polar region form a dome above the star, whereas the ions lifted in the equatorial region form a torus around the star (Figure 7). This equilibrium solution implies no poloidal current and no toroidal magnetic field. We will soon see that these conditions imply that the pulsar does not radiate. The electrosphere formed by lifted from the surface cannot explain the spin-down; however this model is useful to describe old, inactive pulsars. If the magnetosphere is saturated then the charge density can be computed from Equation 8 to give

$$\rho_{GJ} = \varepsilon_0 \boldsymbol{\nabla}\cdot\boldsymbol{E} \approx -2\varepsilon_0 \boldsymbol{\Omega}\cdot\boldsymbol{B} \tag{26}$$

$$= B_0\Omega\left(\frac{R_0}{r}\right)^3 (3\cos^2\theta - 1). \tag{27}$$

Physically, ρ_{GJ} is the charge density required to completely screen the longitudinal electric field. This charge density has the same sign in the vicinity of both magnetic poles (and in fact, the radial vaccum electric field already had the same polarity at both poles). We also note that the lifted charge does not fill the entire magnetosphere: there is a gap between the dome and the torus (Figure 7).

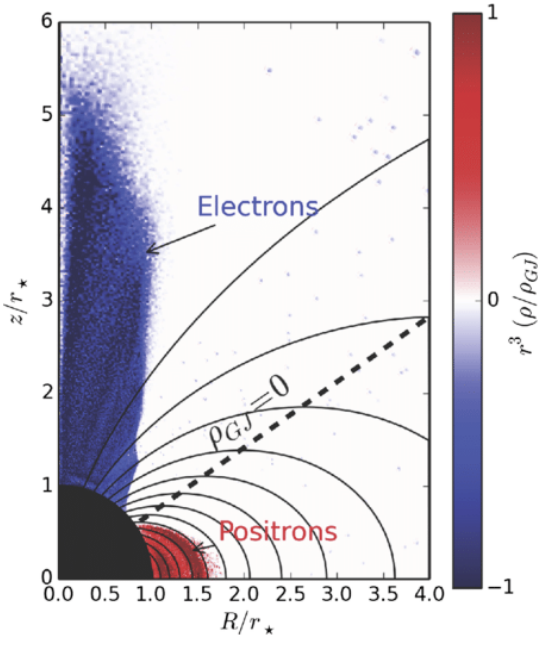

Fig. 7 Electropsphere obtained from a 2D axisymmetric simulation[14] in (R, z) cylindrical coordinates, with $R_{LC} = 6R_0$. Negative charges, in blue, form a dome above the star, whereas positive charges form a torus. The line $\rho_{GJ} = 0$ indicates the gap in the magnetosphere.

Due to the sufficient presence of plasma in the pulsar magnetosphere, its conductivity is high enough so $\boldsymbol{E}\cdot\boldsymbol{B}=0$ is fulfilled: all charged particles adapt their motion to maintain a vanishing acceleration along field lines. Ideal magnetohydrodynamics (MHD) therefore give a suitable description of the magnetospheric plasma (see Appendix 7.2 for more details). In this regime, ideal Ohm's law from Equation 59 reads

$$\boldsymbol{E}+\boldsymbol{U}\times\boldsymbol{B}=\boldsymbol{0}. \tag{28}$$

It is assumed that just like the stellar interior, the plasma surrounding the star is corotating with it, at least close to the light cylinder. The light cylinder is an imaginary cylindrical surface whose axis is parallel to the rotation axis of the star and whose radius is $R_{LC}=c/\Omega$. For usual pulsars $R_{LC}\sim 10^8$ m. Corotation is impossible beyond the light cylinder without the drift speed of the plasma exceeding the speed of light c. It is ensured by the $\boldsymbol{E}\times\boldsymbol{B}$ drift, which does not induce any currents. This drift does not forbid motion along magnetic field lines, so that the drift speed can be written

$$\boldsymbol{U}=\boldsymbol{\Omega}\times\boldsymbol{r}-\frac{\boldsymbol{B}\cdot(\boldsymbol{\Omega}\times\boldsymbol{r})}{B^2}\boldsymbol{B}. \tag{29}$$

In order to avoid exceeding c, field lines must bend, and induce a toroidal component $B_\varphi\neq 0$.[15] So longitudinal currents, which have not been determined so far, are responsible for the toroidal component of $\boldsymbol{B}$.

3.3. Plasma-filled magnetosphere and the force-free approximation

Our model is still dramatically incomplete. First, ideal MHD deals with quasi-neutral plasmas, although we saw that electric screening required charge separation. We cannot be certain the extraction mechanism is sufficient to fill the magnetosphere with plasma. Second, we saw that such a pulsar cannot spin down, which leaves us with our main problem. Besides, observations of pulsar nebulae indicate that the pulsar wind is heavily loaded with electron/positron ($e^\pm$) plasma, which must be created somewhere in the magnetosphere. Creation of $e^\pm$ pairs is also expected theoretically, due to strong electric fields that must develop in the gap (plasma-starved region). Actually, we labeled the extraction of charges from the stellar crust "primary plasma generation" in contrast with the "secondary plasma generation". Since the dipole field lines are curved, the relativistic motion of charged particles along these lines gives rise to curvature radiation, and the emission of γ photons.[13] These emitted photons, propagating in straight lines, cross magnetic field lines.[17] A photon in the vacuum cannot create an $e^\pm$ pair because of the conservation of 4-momentum. However, in the presence of an orthogonal magnetic field the conservation law includes the magnetic field so that 4-momentum conservation can be fulfilled (Figure 8). This stems from the fact that the energy levels of an electron inside a strong magnetic field are quantized (the so-called Landau levels) in increments of $\hbar\omega_c$, where ω_c is the cyclotron frequency. The probability per unit length of conversion of a photon with energy $\epsilon\gg 2m_ec^2$ propagating at an angle θ with respect to the magnetic field $\boldsymbol{B}$ is:[19]

$$p=\frac{3\sqrt{3}}{16\sqrt{2}}\frac{e^2}{4\pi\varepsilon_0\hbar c}\frac{eB\sin\theta}{m_ec}\exp\left(-\frac{8}{3}\frac{B_\hbar}{B\sin\theta}\frac{m_ec^2}{\epsilon}\right), \tag{30}$$

where $B_\hbar=m_e^2c^2/e\hbar$ is the critical field, for which the rest mass of the electron is equal to the energy increment $\hbar\omega_c$. The ratio $B/B_\hbar$ gauges the importance of quantum effects in magnetic fields. This critical field has a value of $B_\hbar=4.4\times10^9$ T, which means that the characteristic magnetic fields of neutron stars are not much smaller than $B_\hbar$. Therefore the neutron star is nontransparent to photons, even with an energy close to the particle creation threshold. This process ignites a cascade of gamma rays and $e^\pm$ pairs until the magnetosphere is saturated.

Now we can be certain the magnetosphere is copiously filled with plasma, so that the particle density is much larger than the minimum required by the corotation. Charge neutrality is insured, the plasma can still be considered as quasi-neutral. Although the existence of gaps is required to fill the magnetosphere with pair plasma, it makes sense to study as a first approximation a situtation in which $\boldsymbol{E}\cdot\boldsymbol{B}\approx 0$. The occurrence of the longitudinal field in some magnetosphere region immediately leads to an abrupt plasma acceleration and the secondary plasma generation, which screens this field. We can study a quasi-stationary situation without explicit time dependence. Besides, the plasma is so magnetized that

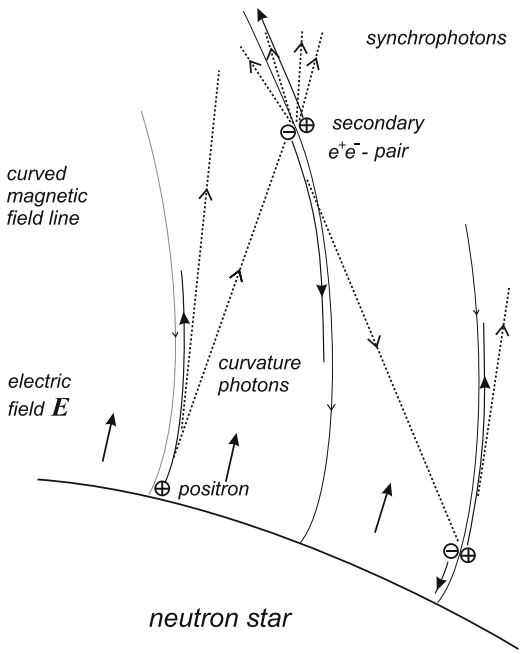

Fig. 8 Particle generation in the vicinity of the neutron star. Primary particles are accelerated by the parallel electric field along curved magnetic field lines and radiate hard γ photons. These curvature photons (in dotted lines) reach the particle generation threshold as field lines are more and more transverse with respect to the photon trajectory. Electron/positron pairs are created, accelerated, igniting the electromagnetic cascade. Figure taken from [17].

the electromagnetic field dominates the dynamics of the plasma with respect to its pressure and inertia (and of course, gravity). Therefore the acceleration of the plasma vanishes which leads to the force-free approximation:[14,15]

$$\rho_e \boldsymbol{E} + \boldsymbol{j} \times \boldsymbol{B} = \boldsymbol{0}. \tag{31}$$

This requires that magnetic energy $B^2/2\mu_0$ dominates any other kind of energy. Moreover no dissipation is associated with this regime and the ideal MHD law can still be applied. The description of the dynamics is completed by Maxwell's equations, connecting the charge density and current density to the fields. The force-free picture does not provide any information about the plasma creation and dynamics however.

4. Solutions in the force-free approximation

In this section, both an analytical and a numerical solution are outlined in the frame of force-free electrodynamics, after deriving the "pulsar equation". The limits of this approach are also underlined.

4.1. Pulsar equation

It is possible to derive a partial differential equation for the electromagnetic field within the force-free model. Since we are interested in axisymmetric configurations, the condition $\boldsymbol{\nabla} \cdot \boldsymbol{B} = 0$ is actually $\boldsymbol{\nabla} \cdot \boldsymbol{B}_P = 0$, where $\boldsymbol{B}_P = (B_r, B_\theta)$ is the poloidal field. Thus there is only one degree of freedom in the poloidal field. We write the total magnetic field as

$$\boldsymbol{B} = \frac{\boldsymbol{\nabla}\Psi \times \boldsymbol{e}_\varphi}{R} + \frac{I}{R}\boldsymbol{e}_\varphi, \tag{32}$$

where $R = r\sin\theta$ is the radial cylindrical coordinate, $\Psi(R,z)$ is the flux function and $I(R,z)$ the current function.[17] This definition is very convenient because:

- $2\pi \mathrm{d}\Psi = \boldsymbol{B}_P \cdot \mathrm{d}\boldsymbol{S}$, so that $2\pi\Psi$ is the magnetic flux through the circle of radius R around the rotation axis at height z;
- $\boldsymbol{B}_P \cdot \boldsymbol{\nabla}\Psi = 0$, so that lines $\Psi(R,z) = \mathrm{cst}$ lie on magnetic surfaces;
- $2\pi I/\mu_0$ is the current flowing through the same circle.

Let us derive an equation for Ψ and I, assuming corotation.[20] The divergence of Equation 28 gives

$$\rho = -\varepsilon_0 \boldsymbol{\nabla} \cdot (R\Omega \boldsymbol{e}_\varphi \times \boldsymbol{B}). \tag{33}$$

Substracting Equation 28 by ρ and substracting Equation 31 yields

$$\boldsymbol{j} \times \boldsymbol{B} = \rho R\Omega \boldsymbol{e}_\varphi \times \boldsymbol{B}. \tag{34}$$

Besides, Maxwell-Faraday equation can be rewritten in the form

$$\mu_0 \boldsymbol{j} = \boldsymbol{\nabla} \times \boldsymbol{B} + \frac{1}{c^2} R\Omega \boldsymbol{e}_\varphi \times \frac{\partial \boldsymbol{B}}{\partial t}. \tag{35}$$

Then we can substitute ρ and $\boldsymbol{j}$ in Equation 34 using Equations 33 and 35, so that

$$\left[\boldsymbol{\nabla} \times \boldsymbol{B} + \frac{1}{c^2} R\Omega \boldsymbol{e}_\varphi \times \frac{\partial \boldsymbol{B}}{\partial t} + \left(\frac{R\Omega}{c^2}\boldsymbol{\nabla} \cdot (R\Omega \boldsymbol{e}_\varphi \times \boldsymbol{B})\boldsymbol{e}_\varphi\right)\right] \times \boldsymbol{B} = \boldsymbol{0}. \tag{36}$$

Since we consider a vector field stationary in the rotating frame one can substitute $\partial/\partial t$ with $-\Omega\partial/\partial\varphi$. Calculating the term between brackets in the previous equation yields

$$\begin{aligned}&\left(\frac{1}{R}\left(1-\frac{R^2\Omega^2}{c^2}\right)\frac{\partial B_z}{\partial\varphi}-\frac{\partial B_\varphi}{\partial z}\right)\boldsymbol{e}_R\\ +\quad&\left(\left(1-\frac{R^2\Omega^2}{c^2}\right)\left(\frac{\partial B_R}{\partial z}-\frac{\partial B_z}{\partial R}\right)+\frac{2R\Omega^2}{c^2}B_z\right)\boldsymbol{e}_\varphi\\ +\quad&\left(\frac{1}{R}\frac{\partial(}{\partial RB_\varphi)}R-\frac{1}{R}\left(1-\frac{R^2\Omega^2}{c^2}\right)\frac{\partial B_R}{\partial\varphi}\right)\boldsymbol{e}_z,\end{aligned}\tag{37}$$

so that Equation 36 can be simplified as

$$(\boldsymbol{\nabla}\times\boldsymbol{B}^*)\times\boldsymbol{B}=\boldsymbol{0},\tag{38}$$

where $\boldsymbol{B}^*$ is given in *cylindrical* coordinates by

$$\boldsymbol{B}^*=\left(\left(1-\frac{R^2\Omega^2}{c^2}\right)B_R,B_\varphi,\left(1-\frac{R^2\Omega^2}{c^2}\right)B_z\right).\tag{39}$$

Then all that is left to do is to plug this equation in Equation 32. It is left to the reader to check that this yields indeed the pulsar equation:

$$\begin{aligned}\left(1-\frac{R^2}{R_{LC}^2}\right)\left(\frac{\partial^2\Psi}{\partial R^2}+\frac{\partial^2\Psi}{\partial z^2}\right)-\left(1+\frac{R^2}{R_{LC}^2}\right)\frac{1}{R}\frac{\partial\Psi}{\partial R}\\ =-I(\Psi)\frac{\partial I}{\partial\Psi}.\end{aligned}\tag{40}$$

It can be shown that if $I=0$, that is, in the absence of longitudinal currents, the field lines are perpendicular to the light cylinder. Consequently, the Poynting vector has no component normal to the light cylinder, and the electromagnetic flux vanishes. If $j_\parallel=0$, then the pulsar does not radiate at all, and we are left with our problem! The energy loss of the pulsar cannot come from currents circulating inside the magnetosphere without crossing the light cylinder. Moreover, the solutions inside and outside the light cylinder are disconnected, the equation being singular at $R=R_{LC}$. A qualitative argument can be underlined as to why parallel currents are necessary to cross the light cylinder.[17] As we already mentioned, magnetic field lines have to bend close to and beyond the light cylinder, to keep the drift velocity from exceeding the speed of light (Equation 29). This will be visible in Section 4.2 when we examine an exact solution of the pulsar equation. Then there is a compensation between the corotation velocity $\boldsymbol{\Omega}\times\boldsymbol{r}$ and the toroidal slide along the magnetic field $j_\parallel\boldsymbol{B}_\varphi/B_\varphi$, so that the drift velocity is directed radially from the star (Figure 9). Thus power can be emitted through the light cylinder.

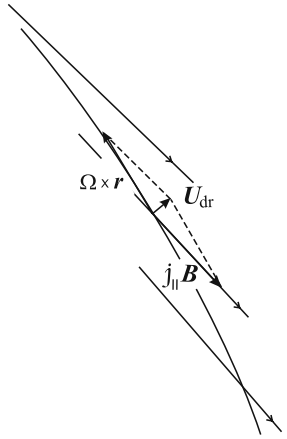

Fig. 9 The drift motion of a charged particle in the presence of a strong toroidal field $B_\varphi\gg B_P$ is nearly radial. Figure taken from [17].

4.2. The split monopole solution

Let us study the features of a particular solution: the split monopole. In the upper hemisphere this solution is given by the flux function $\Psi=\Psi_0(1-\cos\theta)$, equal to the flux of $\boldsymbol{B}$ through a circle of radius R at height z, with $\cos\theta=z/\sqrt{R^2+z^2}$. The associated current function is

$$I(\Psi)=\frac{\Omega}{c}\left(2\Psi-\frac{\Psi^2}{\Psi_0}\right).\tag{41}$$

It is worth giving a consistency check. With this choice for Ψ the current function reads

$$I=\frac{\Omega}{c}\Psi_0\sin^2\theta\ ;\ \frac{\partial I}{\partial\Psi}=2\frac{\Omega}{c}\cos\theta.\tag{42}$$

The terms involving Ψ in the pulsar Equation 40 are given by

$$\frac{\partial^2\Psi}{\partial R^2}+\frac{\partial^2\Psi}{\partial z^2}=-\frac{z}{(R^2+z^2)^{3/2}}=\frac{1}{R}\frac{\partial\Psi}{\partial R}.\tag{43}$$

Inserting this into the the pulsar equation gives the expected result, with $\sin\theta=R/\sqrt{R^2+z^2}$. There only remains to compute the electric and magnetic fields. Using the decomposition of the magnetic field 32 one can write in cylindrical coordinates (r,φ,z):

$$\boldsymbol{B}=\left(-\frac{1}{R}\frac{\partial\Psi}{\partial z},\frac{I}{R},\frac{1}{R}\frac{\partial\Psi}{\partial R}\right),\tag{44}$$

which, in spherical coordinates, yields

$$\begin{cases} B_r = B_0 \dfrac{R_0^2}{r^2} \\ B_\theta = 0 \\ B_\varphi = -B_0 \dfrac{R_0}{R_{LC}} \dfrac{R_0}{r} \sin\theta. \end{cases} \tag{45}$$

This solution is quite simple; the poloidal component is unchanged from an unrotating monopole.[14] The electric field is given by the ideal Ohm's law and reads $\boldsymbol{E} = cB_\varphi \boldsymbol{e}_\theta$, noticing that $B_\varphi = -(U_\varphi/c)B_r$. Interestingly, the toroidal field dominates over the radial field for $r \gg R_{LC}$, in accordance with our previous analysis (Figure 10). Magnetic field lines are spirals that wind up around the pulsar. The solution in the lower hemisphere is obtained via the transformation $\boldsymbol{B} \to -\boldsymbol{B}$, $\boldsymbol{E} \to -\boldsymbol{E}$, to satisfy $\boldsymbol{\nabla}\cdot\boldsymbol{B} = 0$. The reversal of the magnetic field across the equator implies the presence of an equatorial current sheet (Figure 11), which is not accounted by the simple calculation:

$$\boldsymbol{j} = \frac{1}{\mu_0}\boldsymbol{\nabla}\times\boldsymbol{B} = -\frac{2B_0}{R_{LC}}\frac{R_0^2}{r^2}\cos\theta \boldsymbol{e}_r. \tag{46}$$

Plasma is extracted from the star and flows radially outward. The equatorial current sheet ensures that the net current through the stellar surface vanishes, so the stellar charge remains constant. This feature of the solution is very important and will endure in the case of more complex magnetic configurations.

What about energy losses? Since this solution displays longitudinal currents and a magnetic toroidal component, the flux of the Poynting vector through the light cylinder is not vanishing. The radial Poynting vector is $\Pi_r = cB_\varphi^2/\mu_0$, so that the total emitted power is

$$\mathcal{P} = \iint \boldsymbol{\Pi}\cdot \mathrm{d}\boldsymbol{S} = \frac{8\pi B_0^2 R_0^4 \Omega^2}{3\mu_0 c}. \tag{47}$$

One can prove that this result does not depend on the obliquity χ between Ω and the antisymmetry plane of $\boldsymbol{B}$.[21] Eventually we have an aligned rotator that does spin down. Let us highlight an important point: although the plasma energy density is much smaller than the magnetic energy density, its presence is crucially important. The structure of the the fields in the far zone is strongly influenced by the currents the plasma

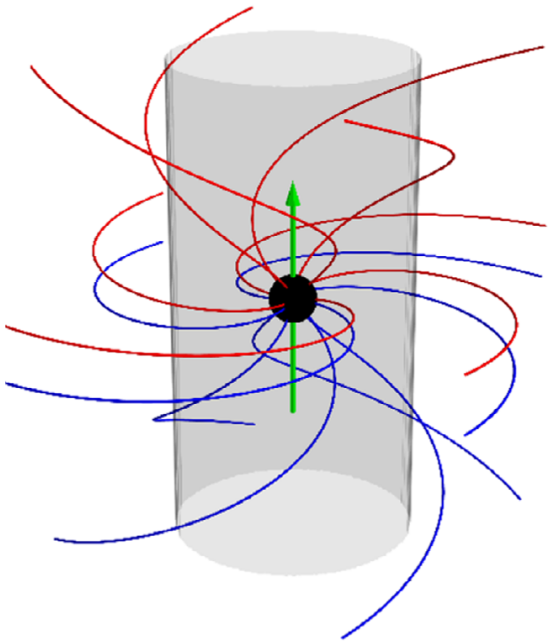

Fig. 10 Magnetic field lines in the analytical monopole solution. The green arrow is the rotation axis. Red lines represent outgoing field lines whereas blue lines are ingoing field lines. The winding up of the field lines around the light cylinder due to the pulsar rotation is visible. Figure taken from [14].

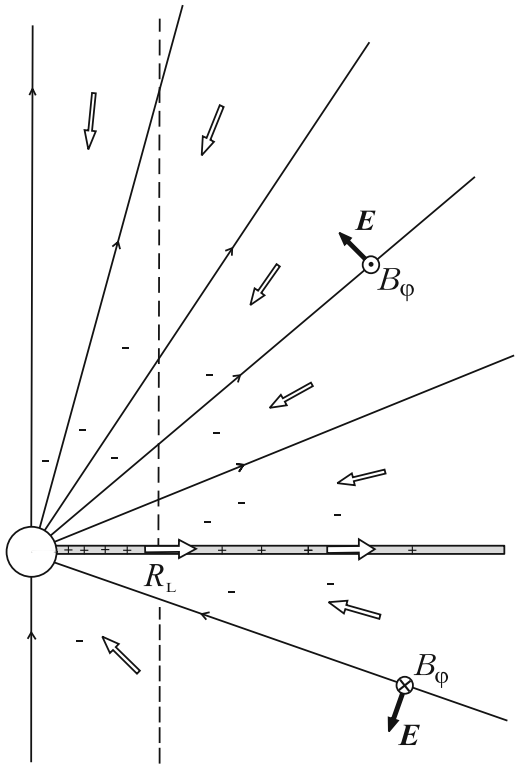

Fig. 11 Features of the split monopole solution. Magnetic field lines are solid black lines, whereas current density is pictured by contour arrows. The current sheet is positively charged. Figure taken from [17].

carries. As the magnetic field is frozen in the plasma, which cannot rotate with superluminal velocity, field lines beyond the light cylinder are wrapped backwards with respect to the rotation star, as indicated by the solution for B_φ. As a result, even an aligned rotator loses energy by driving a plasma wind, provided its magnetosphere is first filled with plasma.

The split magnetic monopole, however unrealistic, is a useful model because far from the cylinder any magnetic configuration will tend to resemble the monopole solution, with a poloidal field that is nearly radial and a dominant toroidal component.

4.3. Magnetospheric structure

Let us now study the more interesting case of a magnetic dipole. At the stellar surface, the flux function has the following boundary condition:

$$\Psi(R_0, \theta) = \frac{\mu_0 \mathcal{M} \sin^2\theta}{4\pi R_0}. \tag{48}$$

No analytical solution is known for the rotating dipole: the pulsar equation for Ψ with the previous boundary condition could not be solved analytically, but was extensively studied numerically.[14] We are going to outline the solution, although some of its features may seem natural after our discussion.

The magnetosphere, presented in Figure 12, is split into two regions. There is a closed zone in which magnetic field lines are closed and look like the dipole field lines. In this zone, the plasma is corotating with the star, with a charge density ρ_e given by Equation 26. Positively charged regions are separated from negatively charged regions by a conical surface with an opening angle defined by the condition $\boldsymbol{\Omega} \cdot \boldsymbol{B} = 0$. In this zone there are no poloidal (longitudinal) currents, and the toroidal field is zero. Since corotation cannot occur beyond R_{LC}, these field lines are necessarily confined in the light cylinder. For a dipole configuration, vacuum field lines are described by the polar equation[12] $r = \lambda \sin^2\theta$ for some constant λ. Thus the last closed field line crosses the stellar surface at the polar angle θ_{pc} given by

$$\sin^2\theta_{pc} \approx \frac{R_0}{R_{LC}}. \tag{49}$$

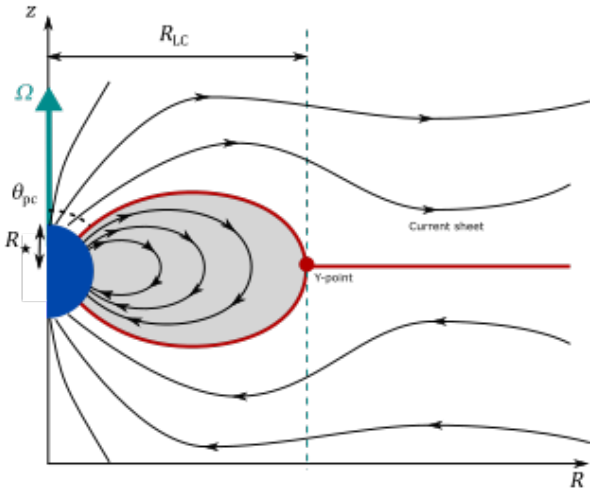

Fig. 12 Magnetosphere of a magnetic dipole neutron star in the force-free approximation. The z axis is both the rotation and magnetic axis. The blue half-disk stands for the neutron star. The grey shaded part corresponds to the closed zone, corotating with the star. The current sheet and the separatrix are represented in red. It splits at the light cylinder into a separatrix enclosing the closed zone and joining the star at the polar cap angle $\theta_{\rm pc}$. Field lines above the separatrix are open outgoing field lines, and open ingoing field lines if they are below. Figure inspired by [14].

Note that this is an approximation. Since a convective current flows inside the closed zone, this increases the effective dipole moment, thus slightly radially inflating the field lines. The field lines emerging from the stellar surface with a polar angle $\theta < \theta_{pc}$ are *open* field lines. This part of the stellar surface is called the "polar cap". The magnetosphere displays an open zone of open magnetic field lines, with non vanishing longitudinal currents and toroidal field. This zone carries away rotational energy from the pulsar. These field lines would be closed if there were no rotation. This effect can be thought of as resulting from the effective inertia of the magnetic field $B^2/2\mu_0$, much greater than the plasma inertia. This stems from the MHD picture: magnetic field is carried away as it is frozen in the plasma. Open magnetic field lines let particles infinitely escape from the pulsar, carrying an electric current Poynting flux and releasing power. The star then loses charges from the polar caps through the formation of a pulsar wind. This also implies that the poloidal magnetic field is ultimately ra-

dial, which justifies why the split monopole solution can be relevant in the far-zone. At the light cylinder, just like in the monopole case, the poloidal and toroidal fields are comparable. In the wind zone, described by ideal MHD, conservation of the magnetic flux in a diverging flow implies that the poloidal field will decrease faster than the toroidal field:[22] $B_R \sim 1/R^2$ and $B_\varphi \sim 1/R$. The last ordering comes from the fact that the number of field lines in the sectional area is constant.

The closed and open zones are separated by a Y-shaped current sheet,[14] that supports the jump in the toroidal magnetic field inside the light cylinder, and the jump $\boldsymbol{B} \to -\boldsymbol{B}$ across the equatorial sheet beyond R_{LC}. To maintain a steady state, plasma must be continuously generated on the open field lines, and the current sheet ensures the net stellar charge remains zero and closes the circuit. Indeed, the total current outflowing from the pulsar surface is to be zero, whereas charges of the same sign are to outflow from both magnetic poles.[17]

This finally makes it possible to physically describe the spin-down of the pulsar.[15,17] Recall that if the pair creation process is sufficiently effective, magnetic dipole radiation will not carry energy away from the pulsar, because the plasma that fills the magnetosphere fully screens any low frequency radiation. The braking mechanism is of another kind (Figure 13). Resulting from the presence of the current sheet, surface currents $\boldsymbol{j}_s$ flow over the stellar surface and experience the Laplace force, which induces a braking torque

$$\boldsymbol{K} = \iint (\boldsymbol{r} \times (\boldsymbol{j}_s \times \boldsymbol{B}))\mathrm{d}S. \qquad (50)$$

The spindown fully results from this torque. This energy $\mathcal{P} = -\boldsymbol{\Omega} \cdot \boldsymbol{K}$ is drawn from the rotational energy and carried away by the electromagnetic flux. Contrary to magnetodipole emission, this loss is realized at zero frequency. This mechanism occurs even for an axisymmetric rotator. For obliquities χ not too close to 90°, the torque is antiparallel to the star magnetic moment. Because the toroidal component of the magnetic field is discontinuous at the stellar surface, the surface currents are given (in spherical coordinates) by

$$\boldsymbol{j}_s = \frac{I}{\mu_0 R_0 \sin\theta}\boldsymbol{e}_\theta. \qquad (51)$$

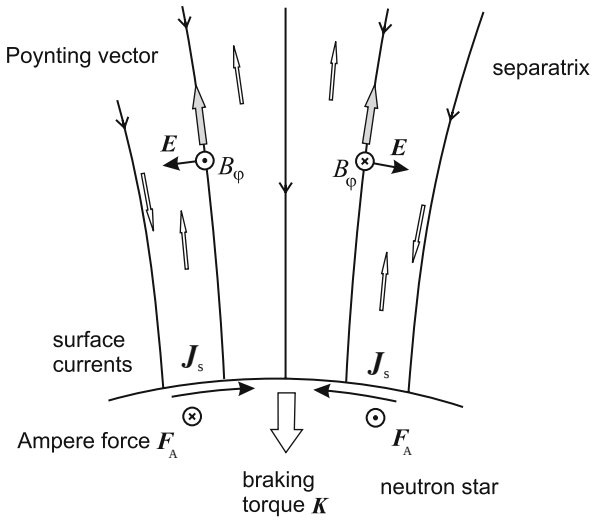

Fig. 13 Orthoradial surface currents $\boldsymbol{j}_s$ flow at the stellar surface. They experience Ampère's force from the toroidal magnetic field, which in turn induces a braking torque $\boldsymbol{K}$ on the star.

This highlights that longitudinal currents are necessary to explain the spin-down of pulsars. Let us estimate the energy loss by the Poynting vector flux through the light cylinder. At the light cylinder, similarly to the monopole magnetosphere, we have $B_\varphi \sim B_P$ and $E_\theta \sim B_P$. The net radial Poynting flux can be estimated as

$$\mathcal{P} \sim \frac{1}{\mu_0} 4\pi R_{LC}^2 E_\theta B_\varphi \sim \frac{4\pi B_0^2 R_0^6 \Omega^4}{\mu_0 c^3}. \qquad (52)$$

This is of the same order of magnitude than the magnetodipole loss from Equation 21, but through a completely different mechanism. Numerical simulations[23] for the inclined rotator showed that the emitted power could be well approximated bythe following formula (Figure 14):

$$\mathcal{P} = \frac{4\pi B_0^2 \Omega^4 R_0^6}{\mu_0 c^3}(1 + \sin^2\chi). \qquad (53)$$

Contrary to the inclined monopole case, the dipole spindown power depends on χ. As mentioned earlier, this dependence on χ does not originate from higher dipole radiation. This problem is investigated in [24]. It originates from the increasing concentration of the open magnetic flux towards the equator in the dipole configuration. Indeed, the Poynting flux reads

$$\Pi_r \sim (\boldsymbol{E} \times \boldsymbol{B})_r \sim E_\theta B_\varphi \sim B_r^2 r^2 \sin^2\theta.$$

The Poynting flux is concentrated at the equatorial belt. In the monopole solution $r^2 B_r$ is a constant everywhere, so the power loss does not depend on χ. For a dipole field however, B_r is greater near the equator than at the poles, which justifies the result (Figure 14).

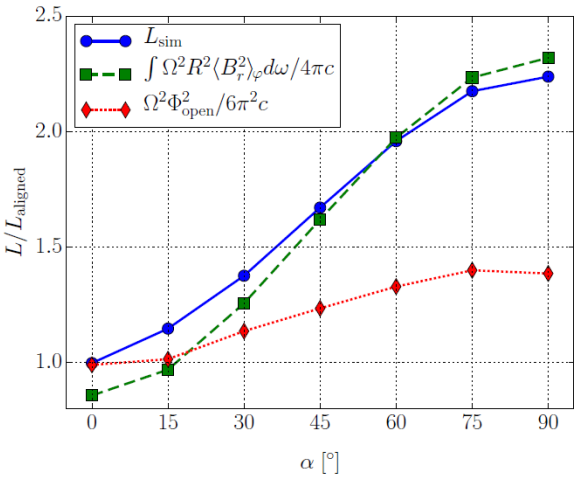

Fig. 14 The blue solid line shows the dependence in th obliquity $\alpha = \chi$ of the spin-down power L (normalized with the aligned rotator luminosity) resulting from a series of simulations. The green dashed line shows the impact of the non-uniformity of magnetic flux, which is likely to explain the dependence of the spin-down power with χ as it quite matches the simulations. Figure taken from [24].

One caveat in that approach remains: the force-free approach is unable to explain particle acceleration, nor quantify the amount of energy transferred to these particles. High-energy radiation is due to the production of ultra-relativistic particles. As an illustration, Figure 15 shows the spectral energy distribution of the Crab pulsar (in black) and the Crab nebula. Pulsar radiation is clearly non-thermal and shows two bumps, which are likely due to the cooling of ultra-relativistic particles through synchrotron radiation and inverse Compton scattering. Particle-in-cell (PIC) simulations can be performed to track particles.[14] It was demonstrated that a prominent site for particle acceleration is the current sheet.[25] Indeed, the force-free and ideal MHD approximations break down in this zone. The mechanism responsible for particle acceleration in the current sheet is magnetic reconnection for reviews of experiments and simulations.[26–28]

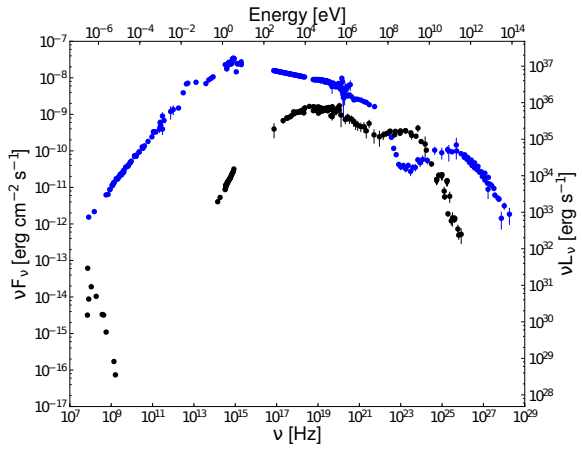

Fig. 15 Spectral energy distribution of the Crab nebula (in blue) and the Crab pulsar (in black). The luminosity shown on the right axis was calculated assuming a distance of 2 kpc. Figure taken from [8].

5. Conclusion

A fascinating aspect in astrophysics is how we are able to deduce some much understanding from so little information. Although pulsars, and in particular the Crab nebula, have provided a wealth of data, it mainly consists in the electromagnetic spectrum of its radiation (granted, in a very wide range of wavelegnths). Yet the nature of pulsars and the structure of its magnetosphere could be elucidated. Because it involves various interplaying phenomena (particle acceleration, pair creation magnetic reconnection, *etc.*), the overall behaviour is still hard to figure out. Force-free elctrodynamics and MHD were able to give a great deal of information as to the spin-down power, and the magnetosphere structure. Now numerical simulations unveil many aspects of pulsar physics. A major challenge rests in the widely different scales, from plasma microphysics (Debye shielding) to the large length scales at play (the pulsar itself and the wind zone). PIC simulations are promising in solving the problem from first principles and have lately been able to predict physical observables.

6. Acknowledgments

I would like to thank Benoît Cerutti for his useful comments on this article. Aside from that, it has been a pleasure to work under his supervision during my internship. This article was written in

the wake of a bibliographic project supervised by Rolf Walder in the last year of my Master's degree at the ENS de Lyon.

7. Appendix

7.1. The electromagnetic drift

A key ingredient of plasma behaviour in magnetic fields is the $\boldsymbol{E} \times \boldsymbol{B}$ drift. Let us consider the movement of a charged particle embedded in constant and uniform $\boldsymbol{B} = B\boldsymbol{e}_z$ and $\boldsymbol{E}$ fields. The parallel component of the electric field will simply accelerate the particle in the $\boldsymbol{B}$ direction, so we will assume $\boldsymbol{E} = E\boldsymbol{e}_x$ and $\boldsymbol{B}$ are perpendicular. The perpendicular equations of motion for a particle with wharge q and mass m in the inertial laboratory frame are

$$\frac{\mathrm{d}v_x}{\mathrm{d}t} = \omega_c v_y + \frac{q}{m}E_x \tag{54}$$

$$\frac{\mathrm{d}v_y}{\mathrm{d}t} = -\omega_c v_x, \tag{55}$$

where $\omega_c = qB/m$ is the cylcotron frequency. Eliminating v_x yields

$$\frac{\mathrm{d}^2 v_y}{\mathrm{d}t^2} + \omega_c^2 \left(v_y + \frac{E}{B}\right) = 0. \tag{56}$$

The solution for this equation corresponds to the usual gyro motion around the magnetic field superimposed to a constant drift both perpendicular to $\boldsymbol{E}$ and $\boldsymbol{B}$:

$$\boldsymbol{v}_\perp(t) = \boldsymbol{v}_{\mathrm{gyro}}(t) + \frac{\boldsymbol{E} \times \boldsymbol{B}}{B^2}. \tag{57}$$

This drift velocity $\boldsymbol{V}_D$ is independent of mass and charge: electrons and ions or positrons drift with the same velocity.[29] We can adress the physical origin of this counterintuitive result. Recall that the gyro radius r_L increases with the perpendicular velocity: $r_L = v_\perp/\omega_c$. Consider for instance the motion of a positive charge. As the particle moves in the direction of the electric field it accelerates, thus inflating its gyro orbit. At some point on its orbit, provided the electric field is not too strong, it will move against the electric field which will decrease its Larmor radius. Consequently, it will return to its original velocity but will have drifted in the perpendicular direction because its Larmor radius has evolved. Since both electric and magnetic parts of the Lorentz force switch signs when we consider a negative charge, the drift will be in the same direction. Therefore the drift does not induce any current, and describes a bulk motion of the plasma (Figure 16).

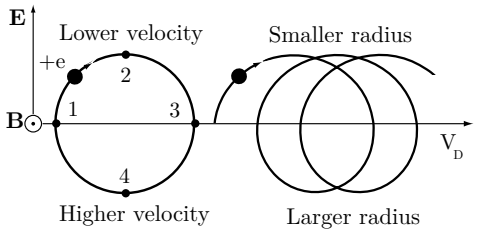

Fig. 16 Effect of an orthogonal electric field on a positive charge. Starting from 1, the charge accelerates until it reaches 2, then turns back if $B > E/c$. It decelerates from 2 to 4. Its gyro-radius is larger at 2 and smaller at 4. Figure taken from [29].

Note that the drift velocity cannot exceed the speed of light, which implies $E < cB$. If this condition is not fulfilled then there is no drift: the electric field is too strong and linearly accelerates the particle. This assertion can be thoroughly demonstrated in the frame of relativistic electrodynamics.[30] The quantity $E^2 - c^2B^2$ can be shown to be Lorentz invariant, so that if there exists an inertial frame in which $E < cB$, it will be so in any inertial frame. Furthermore, there exists an inertial frame in which the electric field vanishes. In classical electrodynamics, this is simply the frame moving with velocity $\boldsymbol{V}_D$ with respect to the laboratory frame. Indeed, in the absence of currents, the transformation law for the electric field is

$$\boldsymbol{E}' = \boldsymbol{E} + \boldsymbol{V}_D \times \boldsymbol{B}, \tag{58}$$

which vanishes according to the expression of the drift (Equation 57). Consequently, in the frame moving at the drift velocity, the plasma experiences no electric field.

7.2. Ideal MHD

In ideal MHD, resistive phenomena occurring in the plasma are neglected. In a nearly perfectly conducting plasma, the electric and magnetic fields are related by the ideal Ohm's law:

$$\boldsymbol{E} + \boldsymbol{U} \times \boldsymbol{B} = \boldsymbol{0}. \tag{59}$$

This will allow us to derive the main feature of ideal MHD: *the magnetic flux through any loop co-moving with the plasma is constant.*[31] This is

the *frozen flux* property. This can be fairly understood since $\boldsymbol{E}' = \boldsymbol{E} + \boldsymbol{U} \times \boldsymbol{B}$ represents the electric field in the reference frame moving with the plasma, in the limit of non-relativistic change of frames. If the magnetic flux were time-dependent, then Faraday's law would imply the existence of an electric field. n order to thoroughly prove this result, let us consider a surface $\mathcal{S}(t)$ bounded by a closed contour $\mathcal{C}(t)$ moving with the plasma. The magnetic flux through $\mathcal{S}(t)$ is

$$\Phi(t) = \iint_{\mathcal{S}(t)} \boldsymbol{B}(\boldsymbol{x}, t) \cdot \mathrm{d}\boldsymbol{S}. \tag{60}$$

Variations of Φ can be due to the explicit time dependence of $\boldsymbol{B}$ or the plasma motion. In the second case, if $\mathrm{d}\boldsymbol{x}$ is an infinitesimal element of $\mathcal{C}$ at time t, then $\boldsymbol{U} \times \mathrm{d}\boldsymbol{x}\delta t$ is the area swept by $\mathrm{d}\boldsymbol{x}$ during time δt, and the magnetic flux through this area is $\boldsymbol{B} \cdot \boldsymbol{U} \times \mathrm{d}\boldsymbol{x}\delta t = \mathrm{d}\boldsymbol{x} \cdot \boldsymbol{B} \times \boldsymbol{U}\delta t$. The rate of change of Φ is therefore

$$\begin{aligned}
\mathrm{d}\Phi t &= \iint_{\mathcal{S}(t)} \partial \boldsymbol{B} t \cdot \mathrm{d}\boldsymbol{S} + \oint_{\mathcal{C}(t)} \mathrm{d}\boldsymbol{x} \cdot \boldsymbol{B} \times \boldsymbol{U} \\
&= -\iint_{\mathcal{S}(t)} \boldsymbol{\nabla} \times \boldsymbol{E} \mathrm{d}\boldsymbol{S} + \iint_{\mathcal{S}(t)} \boldsymbol{\nabla} \times (\boldsymbol{B} \times \boldsymbol{U}) \mathrm{d}\boldsymbol{S} \\
&= -x \iint_{\mathcal{S}(t)} \boldsymbol{\nabla} \times (\boldsymbol{E} + \boldsymbol{U} \times \boldsymbol{B}) \mathrm{d}inguS \\
&= 0,
\end{aligned} \tag{61}$$

in the ideal MHD limit. Note that since magnetic field lines can be regarded as infinitely thin flux tubes, magnetic field lines can be said to be frozen in the plasma, and move with it. Thus magnetic field lines embedded in an ideal MHD plasma can never break or reconnect. This property allows us to justify Equation 7, when we invoked magnetic flux conservation to justify several orders of magnitude as to typical star magnetic fields. The hot plasma constituting stars is conducting enough so ideal MHD can be used in a fairly good approximation. Ideal MHD and Equation 59 will be used extensively in the following.

References

(1) Carroll, B. W.; Ostlie, D. A. , *An Introduction to Modern Astrophysics*, 2nd ed.; Pearson: 2007.

(2) Garing, C., *Ondes électromagnétiques dans les milieux conducteurs*; Ellipses: 1999.

(3) Padmanabhan, T. , *Theoretical Astrophysics, Volume II: Stars and Stellar Systems*; Cambridge University Press: 2001.

(4) Carroll, S. M. , *Spacetime and Geometry: An Introduction to General Relativity*; Pearson: 2003.

(5) Diu, B.; Guthmann, C.; Lederer, D.; Roulet, B., *Physique Statistique*; Hermann: 1996.

(6) Gendreau, K. C.; Arzoumanian, Z.; Okajima, T. In *Space Telescopes and Instrumentation 2012: Ultraviolet to Gamma Ray*, 2012; Vol. 8443.

(7) Basdevant, J.-L.; Spiro, M. , *Énergie nucléaire*; École Polytechnique: 2001.

(8) Bühler, R.; Blandford, R. *Rep. Prog. Phys.* **2014**, *77* .

(9) Pacini, F. *Nature* **1967**, *216* .

(10) Goldstein, H.; Poole Jr., C.; Safko, J. , *Classical mechanics*, 3rd ed.; Pearson: 2012.

(11) Michel, F. C.; Li, H. *Phys. Reps.* **1999**, *318* .

(12) Garing, C., *Magnétisme, Statique, induction et milieux*; Ellipses: 1999.

(13) Jackson, J. D. , *Classical Electrodynamics*, 3rd ed.; Wiley: 1998.

(14) Cerutti, B.; Beloborodov, A. M. *Space Sci. Rev.* **2016** .

(15) Pétri, J. *J. Plasma Phys.* **2016** .

(16) Michel, F. C.; Goldwire Jr, H. C. *Astrophysical Letters* **1970**, *5* .

(17) Beskin, V. , *MHD Flows in Compact Astrophysical Objects: Accretion, Winds and Jets*; Springer: 2010.

(18) Medin, Z.; Lai, D. *MNRAS* **2007**, *382* .

(19) Daugherty, J. K.; Harding, A. K. *Astrophys. J.* **1983**, *273* .

(20) Endean, V. G. *Astrophys. J.* **1974**, *187* .

(21) Bogovalov, S. V. *Astron. Astrophys.* **1999**, *349* .

(22) Kirk., J. G.; Lyubarsky, Y.; Pétri, J. , *The Theory of Pulsar Winds and Nebulae*; Becker, W., Ed.; Springer: 2009; Chapter 16, pp 421–450.

(23) Spitkovsky, A. *Astrophys. J.* **2006**, *648* .

(24) Tchekhovskoy, A.; Philippov, A.; Spitkovsky, A. *MNRAS* **2015**, *12* .

(25) Cerutti, B. *et al.* *MNRAS* **2014**, *16* .

(26) Zweibel, E. G.; Yamada, M. *Annu. Rev. Astron. Astrophys.* **2009**, *47* (1) , 291–332.

(27) Kagan, D. *et al.* *Space Sci. Rev.* **2015**, *191* .

(28) Cerutti, B. *et al.* *Astrophys. J.* **2013**, *770* .

(29) Freidberg, J. P. , *Plasma Physics and Fusion Energy*; Cambridge University Press: 2007.

(30) Gourgoulhon, E. , *Relativité restreinte : Des Particules à l'Astrophysique*; CNRS Éditions: 2010.

(31) Bellan, P. M. , *Fundamentals of Plasma Physics*; Cambridge University Press: 2008.